J. Materials, Conc. Struct., Pavements., JSCE, No. 538/V-31, 227-239, 1996 May

COMPUTATIONAL MODEL FOR REINFORCING BAR EMBEDDED IN CONCRETE UNDER COMBINED AXIAL PULLOUT AND TRANSVERSE DISPLACEMENT

Koichi MAEKAWA [1] and Juneid QURESHI [2]

[1] Member of JSCE, Dr. of Eng., Professor., Dept. of Civil Eng., the University of Tokyo (Hongo 7-3-1, Bunkyo-ku, Tokyo 113, Japan)
[2] Dr. of Eng., Assistant Prof., Dept. of Civil Eng., NED University of Engineering & Technology, Karachi, Pakistan

An enhanced computational model for the prediction of reinforcing bar behavior under the generic condition of axial pullout and transverse displacement is presented. Based on the compatibility relationship between the transverse displacement and the curvature induced in the embedded bar, the localized phenomenon of the bar close to the interface is formulated, and its formulation makes it possible to express the reduced pullout stiffness of embedded bars encountered under combined axial pullout and transverse dowel action.

Key Words: *bond, dowel action, pullout, reinforcement, constitutive law*

1. INTRODUCTION

There exist several constitutive laws which can be combined to formulate plate and joint models for smeared and discrete crack elements for FEM application. In general, these constitutive laws have been verified under simplified loading conditions, and their applicability under generic conditions needs to be checked. The relation between bond stress-slip-strain has been formulated [2] by treating the reinforcement in concrete as a one dimensional cord. This consideration is valid for a single mode deformational path in which the reinforcement is subjected to axial deformation only.

However, when deformational paths are of a mixed mode nature, i.e. axial pullout coupled with transverse displacement, the applicability of the existing model is invalidated in terms of the reduction in the axial stiffness and the mean yield strength of the reinforcement, due to a zone of localized yielding in the reinforcement close to the crack plane, as detailed in reference[16]. The shear capacity of a crack plane, which might govern the ultimate load under specific structural conditions, is therefore not decided by the axial stiffness and strength represented by bare steel bars under uniaxial deformation, but that by the coupled interaction of longitudinal and transverse displacement which is brought about by the equilibrium and compatibility requirements of a crack plane, and cannot be ignored when RC joint plane has small roughness and/or heavy reinforcement ratio[5].

In this paper, an enhanced computational model for the prediction of a reinforcing bar behavior under generic conditions of axial pullout and transverse displacement is presented, based on the relationship between the transverse displacement and the maximum curvature induced in the embedded bar, along with the consideration of the localized phenomenon of the bar close to a crack and interface.

2. PULLOUT OF REINFORCING BARS COUPLED WITH TRANSVERSE SHEAR

A number of previous studies have been done to develop constitutive models for both steel and concrete components separately, but most of them have been verified under simplified and idealized loading conditions. The modeling of reinforcement has been treated by separately considering the two actions of axial pullout and transverse shear and then superposing these behaviors.

Modeling of reinforcement under uniaxial pullout has been proposed by several researchers, who have established microscopic and macroscopic bond models[2),7),8)]. Shima et al.[2)] formulated a constitutive model for bond stress, strain and axial slip considering both microscopic and macroscopic aspects of bond. This model is taken as a frame-work for modification

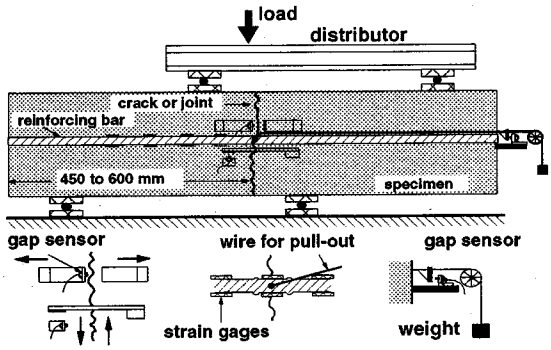

Fig.1 Experimental configuration set-up, instrumentation and loading[16)]

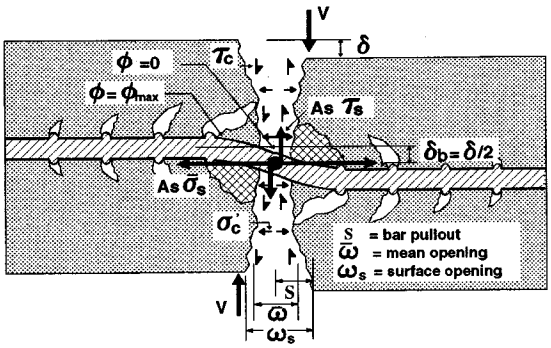

Fig.2 Embedded bar subjected to coupled displacement path.

to propose the enhanced model for embedded bar under generic displacement paths.

Results of tests on embedded bar behavior under loads transverse to the bar axis have been utilized by several researchers to predict the maximum dowel capacity and transverse load - displacement relationships of reinforcement [4),6)]. Nonlinear "beam on elastic foundation" models with variable subgrade stiffness have been proposed but these are limited to reinforcement subjected to transverse loads only, and considerations for bar plasticity or additional damage build-up in concrete, due to radial bond micro cracks originating from the coupled axial loads, as is the condition which reinforcement is subjected to in most RC interfaces, has not been considered.

In the past, prediction for the shear capacity of RC interfaces[5)] was made by the superposition of bar axial bond stress-strain-slip model[2)] with plain concrete stress transfer model[3)]. However, the predictions were not satisfactory [16)], usually resulting in over-estimation of capacity and associated shear displacement when the crack planes are heavily reinforced, even while neglecting dowel contribution by the reinforcing bar. Since the bond-slip-strain model proposed in (2) was formulated under pure tensile conditions, it was presumed that one of the major reasons for the incorrect estimation of shear capacity is the incorrect model for estimating confinement provided by the axial stiffness and strength of the reinforcement under coupled action of crack opening and transverse shear.

To investigate the embedded bar behavior under a coupled displacement path, pure shear loading was adopted in beam type specimens as shown in **Fig.1**[16)]. The shear displacement and associated dilatancy of the shear plane simulates the necessary generic loading path for the embedded bar. By changing either the confining force to the interface, varying the reinforcement ratio, or the shear plane geometry, different displacement paths, applied to the targeted reinforcing bar, were studied. Test results, which are the basis of this study, showed significant decrease in bar axial stiffness and strength, under the coupled displacement paths, compared with the pure uniaxial traction [2)]. Details of the test setup and results can be found in accompanying study in (16).

3. ANALYTICAL MODELING

(1) Mechanical behavior of embedded bar across interface

In a reinforced concrete interface subjected to a shear stress defined as τ_c, a shear displacement, δ, is produced and due to over-riding of the crack surfaces a normal compressive stress, σ'_c, is induced along with an associated normal displacement denoted by ω (crack dilatancy). This normal displacement causes a pullout of the confining embedded steel reinforcement at the interface, S, thereby inducing an axial strain $\bar{\varepsilon}_s$. Also the shear displacement produces a zone of curvature ϕ along the reinforcement close to the interface, with a location where the induced curvature gets maximum as ϕ_{max}. Due to symmetry, the value of curvature is zero at the interface and thus the mean confining steel stress, $\bar{\sigma}_s$, at this location is determined only $\bar{\varepsilon}_s$ induced by the bar pullout.

However, within the curvature influential zone, $\bar{\sigma}_s$ is influenced by both the pullout and the shear slip at the interface owing to three dimensional extent. These parameters which define the deformational and mechanical characteristics of a RC interface are shown in **Fig.2** which stretches the crack width and shear slip for clearly defining the notations. To determine the load deformation relationship and the capacity of the interface, the formulation of embedded bar axial stress under normal and transverse displacement is essential.

(2) Review of bond stress-strain-axial slip model

Shima et al.[2)] proposed a bond stress-strain-axial slip model for reinforcement under uniaxial pullout conditions. The differences in bond-slip relations obtained from pullout tests of long and short

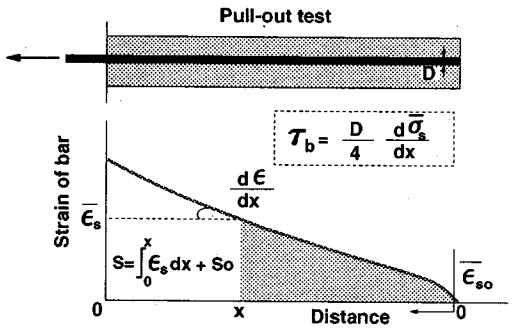

Fig.3 Definitions of local bond stress and slip in model by Shima et al. [2]

embeddments and from axial tension test specimens were expressed by using an unique bond stress-slip-strain relationship, in which the bond stress is formulated as a function of strain multiplied by a function of slip, which is defined as the bond stress when the strain of the bar is zero. The constitutive law for bond stress is given by,

$$\tau_b(\bar{\varepsilon}_s, s) = \tau_{bo}(s) g(\bar{\varepsilon}_s)$$
$$\tau_{bo} = f_c' k\{\ln(1+5s)\}^c \qquad (1)$$
$$g(\bar{\varepsilon}_s) = (1+10^5 \bar{\varepsilon}_s)^{-1}$$

where τ_b is the bond stress, τ_{bo} is the bond stress when bar strain is zero, g is a function depending on bar axial mean strain, $f'c$ is the compressive strength of concrete, s is non dimensional slip = 1000S/D, S is slip, D is bar diameter, and k and c are constants having values of 0.73 and 3, respectively.

For pullout of an embedded bar, the case of interest in the enhanced modeling of the bar and boundary conditions are shown in **Fig.3.**

The equilibrium between bond stress and the mean axial stress is defined by,

$$\tau_b = \left(\frac{D}{4}\right)\frac{d\bar{\sigma}_s}{dx} \qquad (2)$$

The compatibility between axial slip and axial strain is given by,

$$S(x) = \int_0^x \bar{\varepsilon}_s dx + S_o \qquad (3)$$

where, S_o is the slip of the bar at the free end.

This bond stress-slip-strain model, which takes into account effects of bar diameter and concrete strength and is applicable to both the elastic and plastic ranges independent of steel properties, is taken as the framework on which modifications for the proposed model are introduced.

In reference (16), it has been reported that the two new features of bar behavior, which were witnessed experimentally, included (1) the non-uniformity in the distribution of mean strains close to the crack plane, with some extreme fibers in the reinforcement reaching plastic strains at some particular sections while the mean strain at the interface and other points away from the interface were found to be elastic even up to ultimate loads, and (2) the curvature induced in the bar due to the transverse shear displacement is also non uniform with zero curvature at, and some distance away from, the interface. The mean stresses in the reinforcement close to the crack plane, however, showed rather uniform nature.

(3) Proposals for model considering localized effects

In view of the 'localized effects' of the bar behavior close to the interface, two basic proposals, considering the different stress and deformational fields to which the bar is subjected to near the interface, are postulated as below.

a) Zone of Bond Deterioration: In the original pullout tests carried out to formulate the bond stress-strain-axial slip model, an unbonded zone was placed near the loaded surface to ensure uniform bond over the whole reinforcement[2]. However, the bond performance near the real interface may easily be deteriorated due to the splitting and crushing of concrete around the bar. In order to consider this effect, a 'Bond Deterioration Zone' is defined as L_b, the range of which is a function of bar diameter, i.e. $L_b = L_b(D)$. For the computational model L_b is taken as '5D', but not less than the 'Curvature Influencing Zone', as discussed later. The degradation for the bond stress along this zone is proposed by a simple bi-linear function as expressed below.

$$\tau_b(x) = \tau_{b,\max} - \frac{\tau_{b,\max}}{L_b}\{x-(L_e-L_b)\}$$
$$(L_e - L_b \le x \le L_e - L_b/2) \qquad (4)$$
$$\tau_b(x) = 0 \quad (L_e - L_b/2 \le x \le L_e)$$

where $\tau_{b,max}$ is the maximum bond stress attained at the origin of L_b. L_e is the bar embedded length. The bond stress profile along the embedded length, including the newly introduced profile for the concept of a bond deterioration zone, is shown in **Fig.4**.

The concept of a bond deterioration zone has been adopted by considering a linear degradation of bond stress from the origin of bond deterioration zone to the crack surface[12]. The profile adopted here, where bond

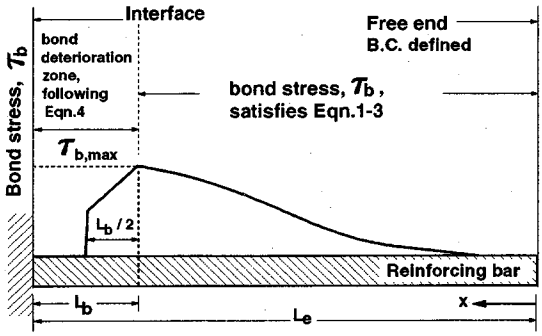

Fig.4 Bond stress profile along embedded bar with deterioration of bond close to the interface.

stress drops to zero after some finite length of the deterioration zone, is to represent the locus from which the radial bond micro-cracks would reach the surface of the interface plane and τ_b would decrease rapidly. It should be noted however that as long as a bond deterioration zone of appropriate size is considered, the profile of degradation is not a very highly sensitive parameter.

In the present model, the integration of the strain profile is carried out over the entire embedded length, L_e, to find the loaded end slip. Within the Bond Deterioration Zone, L_b, the mean axial strain, $\bar{\varepsilon}_s(x)$, is a function of the mean axial stress, $\bar{\sigma}_s(x)$, which in turn is computed from the pre-defined bond stress profile, $\tau_b(x)$, within the zone, i.e.,

$$S = \int_0^{L_e - L_b} \bar{\varepsilon}_s(x)dx + \int_{L_e - L_b}^{L_e} \bar{\varepsilon}_s(\tau_b(x))dx + S_o \qquad (5)$$

Thus, the quantitative effect of the deterioration of bond on the additional pullout of the bar can be obtained, irrespective of long or short embedded lengths.

b) Zone of Curvature Influence: To consider the effect of the localized curvature in the bar, close to the shear plane, the concept of a 'Curvature Influencing Zone', L_c, is introduced. In the tests L_c was observed to be between '4D' and '5D' initially, with a small increase of '1D' to '2D', with increasing load, as shown in **Fig.5**. For the model, the initial zone size, L_c ($=L_{co}$), at small displacements when both materials can be considered to behave elastically, is idealized by considering the bar behavior analogous to a beam on an elastic foundation (BEF), which gives,

$$q = -(kD)\delta_b \qquad (6)$$

where δ_b is the local downward deflection of the supporting concrete foundation under the bar, q is the downward (and -q is the upward) force per unit length of the bar, and k is the foundation modulus taken as constant over the bar diameter, D. Using the classical beam equation, and substituting Eq.(6), we have,

$$\frac{d^4\delta_b}{dx^4} + \frac{(kD)}{E_s I_b}\delta_b = \frac{p'}{E_s I_b} \qquad (7)$$

where p' is any external linear downward load acting on the bar, and E_s and I_b are the elastic modulus and moment of inertia of the bar section, respectively.

Since the embedded bar is not subjected to any external linear load, therefore the 'reduced', (p'=0), general solution of the above equation yields,

$$\delta_b = \exp(\beta x)(C_1 \cos\beta x + C_2 \sin\beta x) + \exp(-\beta x)(C_3 \cos\beta x + C_4 \sin\beta x) \qquad (8)$$

$$\text{where} \quad \beta = \sqrt[4]{\frac{kD}{4 E_s I_b}}$$

If the origin of x is taken at the shear plane interface, and defined as x', the constants of integration can be worked out from the boundary conditions at the two ends for an embedded bar of semi-infinite length subjected to only an external shear force V at the interface with zero bending moment M(=0), i.e.,

$$\begin{aligned} &At \;\; x' \to \infty, \;\; \delta_b = 0 \;\; (C_1 = C_2 = 0) \\ &At \;\; x' = 0, \;\; E_s I_b \delta''_b = M = 0 \\ &\text{and} \;\; E_s I_b \delta'''_b = V \end{aligned} \qquad (9)$$

The solution of differential equation yields,

$$E_s I_b \delta_b{}''' = V\{\exp(-\beta x')(\cos\beta x' - \sin\beta x')\} \qquad (10)$$

Then, the location of the maximum bending moment, and consequently of maximum curvature, x_c', from the interface, is given by,

$$x_{c'} = \frac{\pi}{4}\sqrt[4]{\frac{4 E_s I_b}{kD}} \quad at\, E_s I_b\, \delta''' = 0 \qquad (11)$$

For the model, L_{co} is taken as three times the size of the location of the maximum bending moment, as would be derived from BEF analogy, to give,

$$L_{co} = \frac{3\pi}{4}\sqrt[4]{\frac{4 E_s I_b}{kD}} \qquad (12)$$

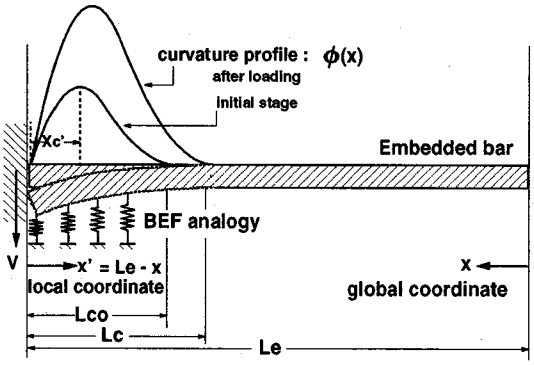

Fig.5 Location of maximum bending moment and size of curvature zone.

$$where \left[k = \frac{150 f_c'}{D} \left(\frac{MPa}{mm^3} \right) \right]$$

The definitions of x'_c and L_{co} are illustrated in **Fig.5**, along with the conceptual variation of the curvature profile, as seen in test results.

Here it is important to mention the equivalence and difference between the 'curvature distribution based model' and the 'beam on elastic/inelastic foundation model'. It is possible to originate from the inelastic reaction model from the concrete foundation, based on which the curvature profile may be derived. In this case, however the model becomes complex and it becomes necessary to consider the difference in bearing reaction along the bar axis at different locations, away from the interface. This factor cannot be directly measured through the experimental approach, with the presence of the contacting concrete surface on the opposite side. Furthermore, since the bearing reaction in the supporting concrete develops from the transverse displacement of the embedded bar, the relaxation of the contact pressure due to localized yielding of the bar is difficult to be modeled through this approach.

Therefore, it was decided to start the computations from the profile pattern of the curvature and the size of the influencing zone, which are directly observed from the experiments. This approach is similar to the method used by Izumo et al.[10] for modeling the tension stiffening behavior in reinforced concrete, based on a trigonometric function for the pattern of the tensile stress profile of main reinforcing bars embedded in concrete. The main advantage of the adopted approach is that reliable experimental data, which is not of a microscopic basis but of a macroscopic one, but which is closely associated with the microscopic fundamentals of transversely supported reinforcing bar, can be the basis for the model.

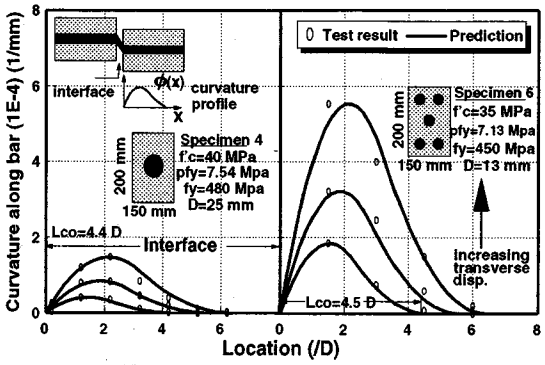

Fig.6 Test [16] and predicted profile of curvature distribution along bar axis for a typical specimen.
p : reinforcement ratio, fy : yield strength

The BEF analogy has been basically utilized for computing the location of the initial maximum bending moment, based on the parameters which influence the curvature zone, since test results of curvature profiles for a wide range of variation of these parameters are not available.

However, for reasons detailed above, the BEF analogy cannot be considered reliable in the later stages of bar pullout and shear displacement, since both the embedded bar and the supporting concrete would behave nonlinearly. As seen in the test results[16], there is a small shift of the curvature influencing zone, with increased shear displacements. The mechanical meaning of this shift is a reflection of the inelasticity of the reaction spring properties, because the inelasticity relaxes the moment localization. The variation of the influencing zone is basically associated with the local crushing or high inelasticity of the reacting concrete near the interface. This gradual softening in the supporting concrete due to increasing bar shear displacements, δ_b, and radial micro bond cracks from bar pullout, S, is modeled by considering an increase in L_c, as a function of L_{co} and a non-dimensional damage build-up parameter, DI, as expressed below,

$$\begin{aligned} DI &= (1 + 150\, S / D)\, \delta_b / D \\ L_c &= L_{co} \qquad (for\ DI \le 0.02) \\ L_c &= L_{co}\{1 + 3(DI - 0.02)^{0.8}\} \\ &\quad (for\ DI > 0.02) \end{aligned} \tag{13}$$

The shape of the curvature distribution, $\phi(x)$, within L_c is modeled by a skewed parabolic form, which conforms well with the curvature profile seen in test results[16], as shown for a typical specimen in **Fig.6**, and is expressed as below,

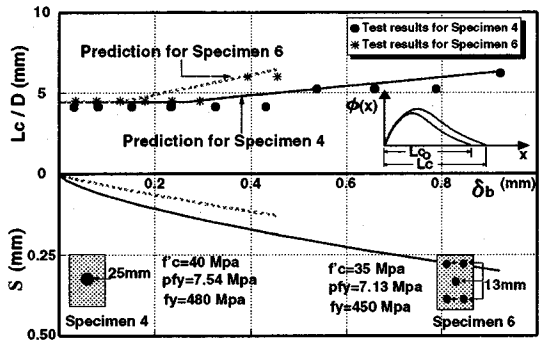

Fig.7 Comparison of predicted and test results of variation of curvature influencing zone under coupled displacement path, for typical specimens.

$$\phi(x) = \frac{3\phi_{max}[x-(L_e-L_c)]^2}{L_c^2}$$
$$for \quad L_e - L_c \le x < L_e - L_c/2$$
$$\phi(x) = -3\frac{\phi_{max}}{L_c^2}[3\{x-(L_e-L_c/2)\}^2 - L_c\{x-(L_e-3L_c/4)\}] \qquad (14)$$
$$for \quad L_e - L_c/2 < x \le L_e$$

The comparison of variation of L_c with test results, of a few typical specimens, is shown in **Fig.7**.

The size of the curvature influencing zone and the shape of the curvature profile, are modeled primarily to reproduce the curvature profiles observed in test results. The expression for the underlying concrete subgrade stiffness, *k*, is within the range of values of *k* adopted in literature by different researchers, as summarized by Poli et al.[4]. Eq.(12), derived from the BEF analogy is a convenient expression to model the zone size based on all the relevant affecting parameters, i.e. bar size, and concrete and steel stiffnesses. Prediction of bar axial and transverse stresses for tests conducted for this study and available data from literature, as will be shown on a later section, validates the modeling of the subgrade stiffness along with the zone size and shape, for sufficiently wide variation of the affecting parameters. The direct verification of zone size and shape with test data of experiments conducted for this study was also done, as shown in **Fig.6** and **Fig.7**.

(4) Compatibility between bar transverse displacement and curvature distribution

Using the classical beam theory assumptions, compatibility conditions require that the sum of the double integral of the curvature distribution, $\phi(x)$, and the integral of the transverse shear deformation, $\gamma(x)$, along the bar axis, must equal the displacement of the bar normal to that axis, $\delta_b(x)$. Satisfying boundary and continuity conditions, we have,

$$\delta_b = \iint_{L_c} \phi(x)\,dx + \delta_{bs}$$
$$\delta_{bs} = \int_{L_e} \gamma(x)\,dx \qquad (15)$$

where, L_c indicates the size of curvature influencing zone, the integrals over which gives the transverse displacement of the bar at the interface, which by compatibility becomes half of the shear displacement of the interface, δ as shown in **Fig.2**.

This geometric compatibility, which holds true irrespective of bar elastic and plastic behaviors, is one of the key relations in the computational model. Once the bar transverse displacement, δ_b, is known, the curvature profile, $\phi(x)$, can be computed and the axial and transverse stresses in the embedded bar can be calculated, due to the coupled action of axial pullout and transverse displacement.

The force system acting on the embedded bar, due to the displacement path at the interface, which will be discussed in detail in the next section, produces insignificant shear deformation of the bar at the interface. Due to the imposed boundary conditions at the ends of the curvature influencing zone, i.e. the origin and the interface, the bending moments must be zero. The profile of the shear force acting on the bar therefore follows a positive and negative contour. Under elastic conditions, the transverse bar displacement due to the shear deformation only, δ_{bs}, can be expressed as,

$$\delta_{bs} = \frac{\alpha}{GA_s}\int_{L_e} V(x)dx = \frac{\alpha}{GA_s}\int_{L_e} dM \qquad (16)$$

where, α is a shape factor which is a function of the shear stress distribution in the cross section, *G* is the shear modulus of elasticity and A_s is the cross sectional area.

Due to the boundary conditions, as mentioned above, the difference in bending moment across L_c must be zero. Therefore, shear deformation under elastic conditions can be considered as non-existent. After the localized yielding of the outer fibers of the bar, due to the curvature, the plasticity proceeds on both sides of the maximum curvature location, i.e. encompassing both positive and negative shear force regions, and the additional shear deformations at the interface location due to the loss of shear rigidity close to the interface are also mostly balanced between these two regions. In view of this behavior, in general, the effect of shear displacement is not considered in the

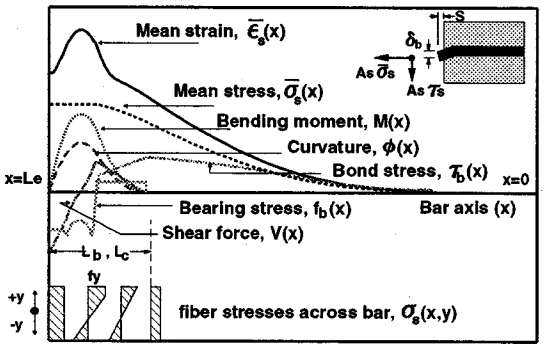

Fig.8 Graphical distribution profiles of typical computed parameters.

computational model. Verification with test results also indicates that by considering only the transverse displacement due to bending rotations, the normal displacement of the bar at the interface can be predicted satisfactorily, as shown in later sections.

(5) Stresses, strains and system of forces acting on embedded bar modeled as 2-D cord

From the assumed distribution profiles of bond stresses and curvature, computations can be carried out for the sectionally averaged mean bar stresses and strains along the bar axis, $\bar{\sigma}_s(x)$ and $\bar{\varepsilon}_s(x)$, respectively, the local stresses and strains along the bar cross section, $\sigma_s(x,y)$ and $\varepsilon_s(x,y)$, respectively (where y is the local coordinate, the origin of which is the centroid of the section concerned), and the system of forces, including axial force P(x), bending moments M(x), shear forces V(x) and contact pressure below the bar $f_b(x)$, along the bar axis. The discretized bar local stresses, $\sigma_s(x,y)$, are computed from the uniaxial stress-strain relationship of bare steel bar[2]. Using the relationships between the mean axial bar stresses and strains with the local stresses and strains, i.e,

$$\bar{\sigma}_s(x) = \frac{\int_{-D/2}^{D/2} \sigma_s(x,y)\,dA_s(y)}{A_s}$$
$$\bar{\varepsilon}_s(x) = \frac{\int_{-D/2}^{D/2} \varepsilon_s(x,y)\,dA_s(y)}{A_s} \qquad (17)$$

where, D is the bar diameter. The governing equations are detailed below.

$$\bar{\sigma}_s(x) = \frac{4}{D}\int_0^x \tau_b(x)\,dx$$
$$\text{where } \tau_b(x) = \tau_b(x, \tau_{b,\max}) \qquad (18)$$
$$(L_e - L_b \le x \le L_e)$$

which is the general equation obtained by integrating Eq.(2). The mean axial bar strain is then computed from $\bar{\sigma}_s(x)$ and $\phi(x)$,

$$\bar{\varepsilon}_s(x) = \bar{\varepsilon}_s(\phi(x), \bar{\sigma}_s(x))$$
$$L_e - L_b \le x \le L_e \qquad (19)$$

$$\text{where } \bar{\sigma}_s(x) = \int_{-D/2}^{D/2} \sigma_s(\varepsilon_s)\,dA_s(y) / A_s$$
$$\text{and } \varepsilon_s = \bar{\varepsilon}_s(x) + \phi(x)\cdot y \qquad (20)$$

The system of forces acting on the bar, are then computed as below,

$$P(x) = \bar{\sigma}_s(x) A_s \qquad (21)$$

$$M(x) = \int_{-D/2}^{D/2} \sigma_s(x,y)\cdot y\,dA_s(y) \qquad (22)$$

$$V(x) = \frac{dM(x)}{dx} \qquad (23)$$

$$f_b(x) = \frac{dV(x)}{dx}\cdot\frac{1}{D} \qquad (24)$$

The effect of the shear stress, τ_s, due to the bending curvature, on the yield stress of the bar is taken into consideration by applying the Von-Mises yield criterion, as below.

$$f_y'(x) = f_y\sqrt{1 - 3(\tau_s(x)/f_y)^2} \qquad (25)$$

by which the reduced mean yield stress, f'_y, for checking the fiber stress state of the bar is obtained.

By solving a) bond constitutive model in Eq.(1-4) simultaneously with b) compatibility conditions with respect to transverse shear displacement and force in Eq.(13-15) and c) equilibrium on sectional forces in Eq.(17-25), we have the coupled effect of pullout and dowel actions. The spatial distribution profile of the computed parameters obtained by simultaneously solving Eq.(1-5) and Eq.(13-24) along the bar axis are shown in **Fig.8**. Also shown are the profile of fiber stresses across the bar section along the 'Curvature Influencing Zone'.

(6) Ultimate axial force criterion for embedded bar

The ultimate axial force provided by the reinforcement under a coupled displacement path, giving rise to interacting bending, shear and axial forces on the embedded bar, can be derived on the

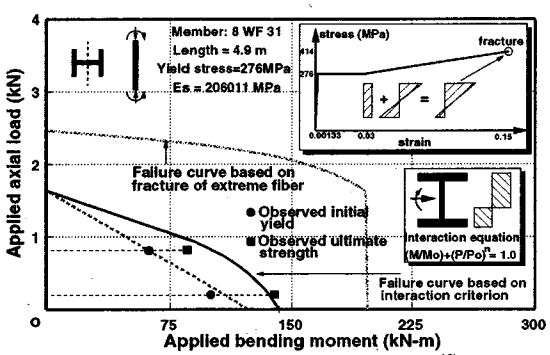

Fig.9 Interaction criteria with test results [13)]

basis of the maximum possible interactive stresses in the bar under such conditions. Using the plane section theory of beams, and idealizing the material stress-strain behavior as rigid plastic with capacity equal to the bar axial yield capacity, the solution of two equilibrium conditions for a given cross section, i.e.,

$$\int_{-D/2}^{D/2} \sigma_s(x,y)\,dA_s(y) = P(x)$$
$$\int_{-D/2}^{D/2} \sigma_s(x,y)\cdot y\cdot dA_s(y) = M(x) \qquad (26)$$

gives the interaction equation in terms of ratios of actual forces to the strength of the section under pure axial and bending forces [13)].

$$\frac{M(x)}{M_o}+\left(\frac{P(x)}{P_o}\right)^2 = 1 \qquad (27)$$

Extending this relation to consider the effect of sectional shear forces, according to the Von-Mises criteria for combined axial and shear forces, we can obtain,

$$\lambda(x) = \left[\frac{M(x)}{M_o}+\left(\frac{P(x)}{P_o}\right)^2\right]^2+\left[\frac{V(x)}{V_o}\right]^2 \qquad (28)$$
$$\lambda(x) = 1$$

where, M(x), P(x) and V(x) are the actual bending moment, axial force and shear on a section, respectively; M_o ($=f_y D^3/6$), P_o ($=A_s f_y$) and V_o ($=A_s f_y/\sqrt{3}$) are the corresponding ultimate capacities under non interactive force conditions. Under any combination of the interacting stresses, when the limit criteria expressed by $\lambda(x)$ equals unity, it implies the ultimate bar axial stress, unless there is a reduction in the other interactive forces.

The experimental verification for deriving such a interaction failure criteria as λ (x), based on the plane section theory, is shown in **Fig.9**. Test results for the ultimate capacity of the section concerned, subjected to combined axial thrust and bending moment[13)], without the problem of instability, were analyzed by two different approaches. The first was the interaction criteria, as described above, and the second was by considering failure to occur when the extreme bar fiber reaches fracture, as defined by the axial stress-strain relation of the bar, under increasing bending moments and a constant axial force. (Since the actual stress-strain relation of the steel section is not mentioned in (13), a typical such relation for a steel with similar yield stress was utilized[15)]). It can be seen from **Fig.9**, that satisfactory predictions of ultimate capacity can be obtained using the interaction criteria, whereas the second approach overestimates the rest data. Similar verification of the interaction equation for test results of hollow rectangular box sections subjected to bi-axial moment and axial tension, without problems of instability, can be found in (14).

4.VERIFICATION OF PROPOSED MODEL

(1) Curvature-shear slip relation

Since the basic compatibility proposal in the model relates the curvature distribution with the shear slip of the reinforcement, the comparison of experimentally measured and computed shear slips of bar, from Eq.(13-15) neglecting shear deformation (δ_{bs}=0), using the experimentally obtained maximum bar curvature, is shown in **Fig.10** for some typical specimens. Satisfactory correlation can be observed, with considerable variation in maximum bar curvature for different specimens. This verification further confirms, as mentioned earlier, that plastic shear deformations are not significant in coupled displacement path tests till the maximum bar axial capacity is attained.

(2) Bar axial stress-pullout relation at interface

Verification of the bar stiffness and strength is done by testing reinforced crack and joint planes, as explained in the test setup as shown in **Fig.1**, which introduces the coupled displacement path for the embedded bar. Testing was carried out for different shear plane geometrical types (processed, P, and unprocessed, U, construction joints, CJ, and rough cracks, RC) and material properties (normal concrete, NC and High Performance Concrete, HPC), along with different reinforcement ratios[16)]. These define unique coupled displacement paths according to the equilibrium and compatibility conditions at the interface.

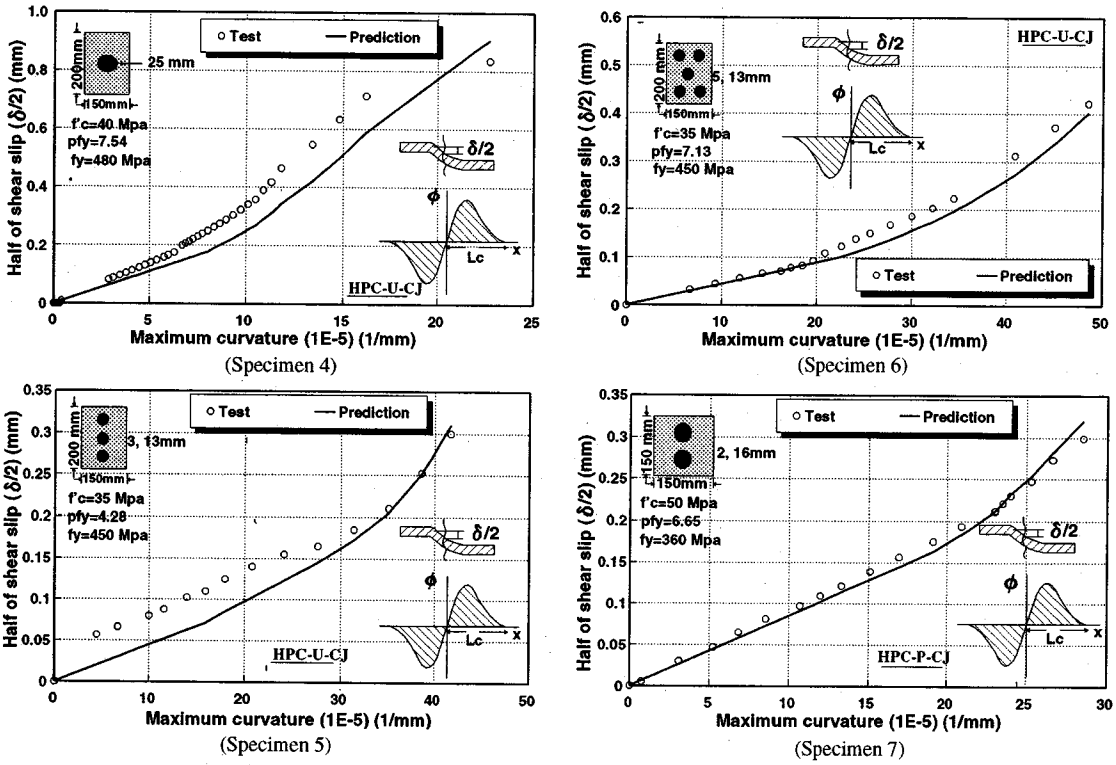

Fig.10 Comparison of experimental [16] and predicted results of compatibility relation between curvature and transverse displacement of bar, for typical specimens.

The test and computed steel axial mean stress versus the pullout and associated transverse displacement at the interface are shown in **Fig.11.** The mean axial stress versus strain results for a similar test specimen[1], at the maximum curvature location, is shown in **Fig.12**. Pure axial pullout results are also shown for comparison, in all the figures. The dotted line with arrow head succeeding the coupled path prediction line, in the figures, indicates the point at which the limiting interactive force criterion, $\lambda(x)$, attains unity. Further increase in displacement path would produce plastic deformations without increase in the axial stress, since the bending moment does not decrease with the increase in bar transverse displacement. The critical location along the bar axis where the limit interactive force criterion is attained is always at the maximum curvature location inside concrete, where the maximum bending moment and axial force exist and shear is none.

This results in the formation of a plastic hinge, since additional bending moments cannot be supported and a possible rotational mechanism develops in the bar between the maximum curvature location and the interface, resulting in loss of the axial restraining force to the interface.

The satisfactory correlation for the initial part of the steel stress-pullout relation, before localized yielding, verifies the first proposal of the model regarding the quantitative effect of the profile of the 'Bond Deterioration Zone', which explains the increased pullout, as compared to uniaxial pullout of the original model with bond deterioration suppressed.

After the localized yielding of the extreme bar fibers, the mean strain profile would become nonuniform, because of the induced curvature, since the mean stress profile is uniform near the crack. Since the integral of the mean strain along the bar represents the pullout of the bar, this non uniformity in the mean strain profile would be the source of the additional pullout, for a given mean stress level, observed in coupled displacement path tests as compared to uniaxial pullout tests. The prediction of the non-linear part in the steel stress-pullout relation verifies the second proposal in the model regarding the quantitative effect of the 'Curvature Influencing Zone'. In consideration of the limiting value of the interactive stresses possible at the maximum curvature location, due to combined axial and bending stresses, the ultimate axial force of the bar can also be predicted satisfactorily, (**Fig.11** and **Fig.12**).

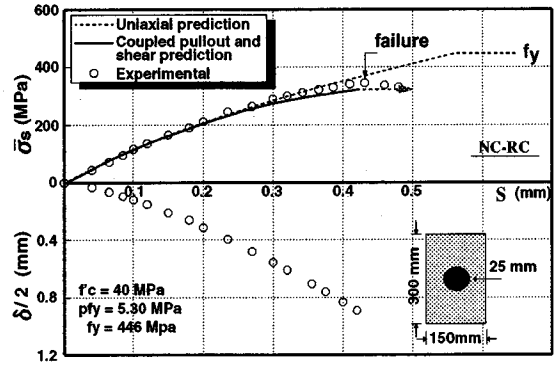

(Specimen 1)

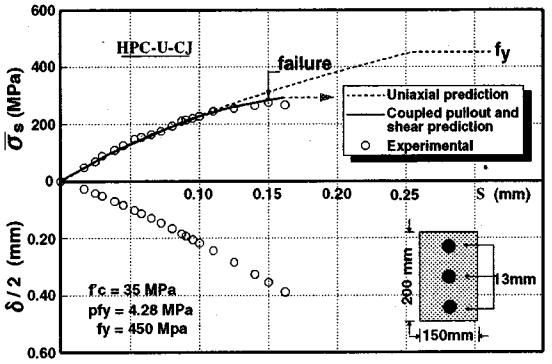

(Specimen 5)

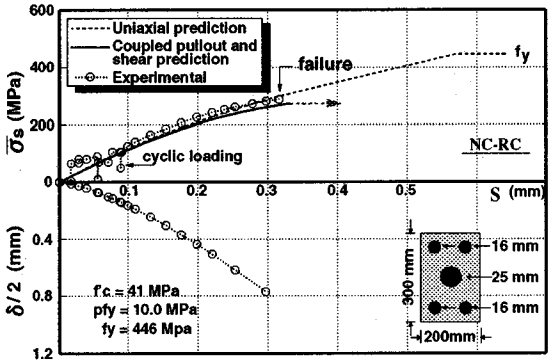

(Specimen 2)

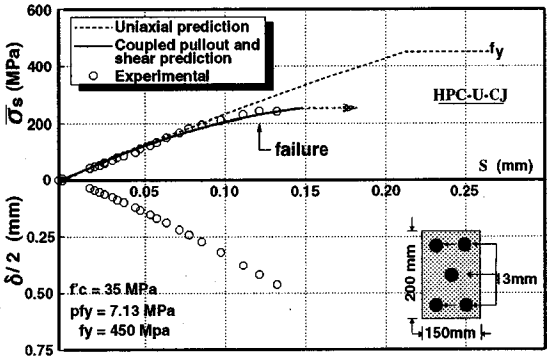

(Specimen 6)

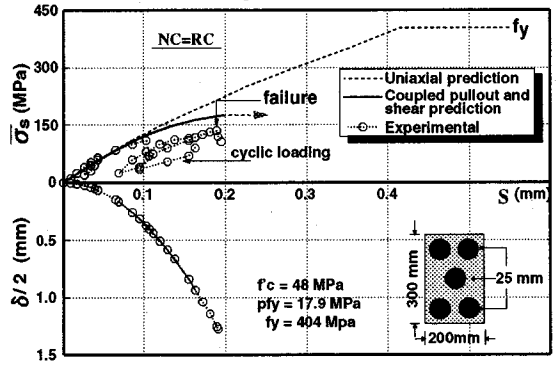

(Specimen 3)

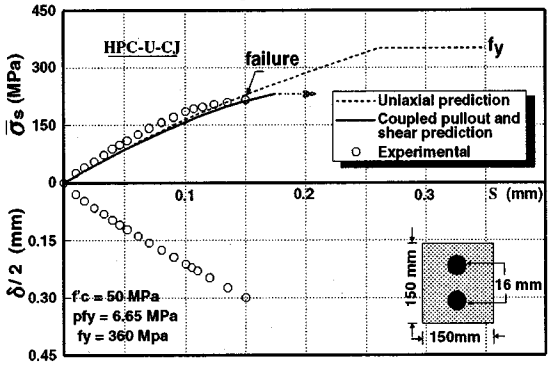

(Specimen 7)

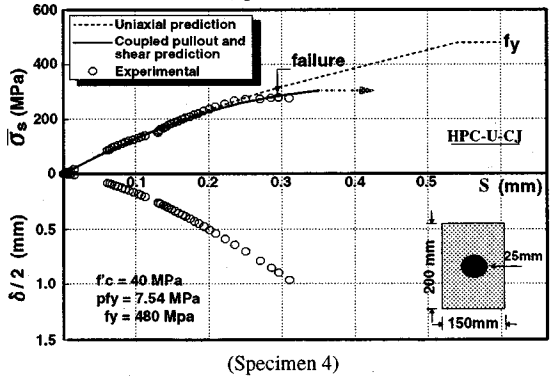

(Specimen 4)

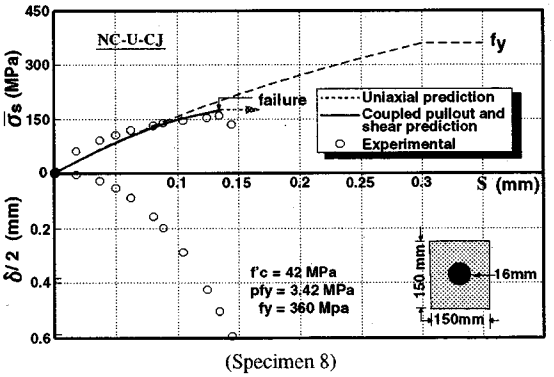

(Specimen 8)

Fig.11 Comparison of experimental [16] and predicted mean axial bar stress, at failure of specimens, and associated displacement path at the interface.

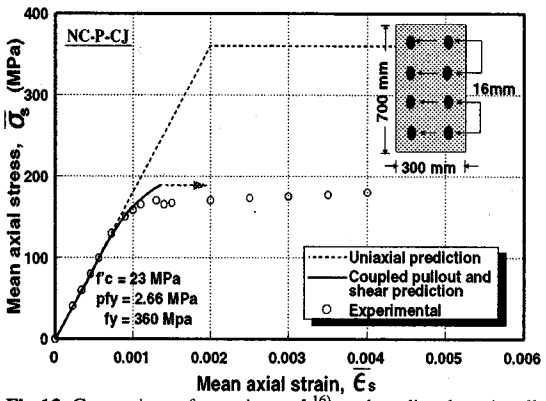

Fig.12 Comparison of experimental [16] and predicted sectionally averaged mean axial stress and strain at maximum curvature location [1]

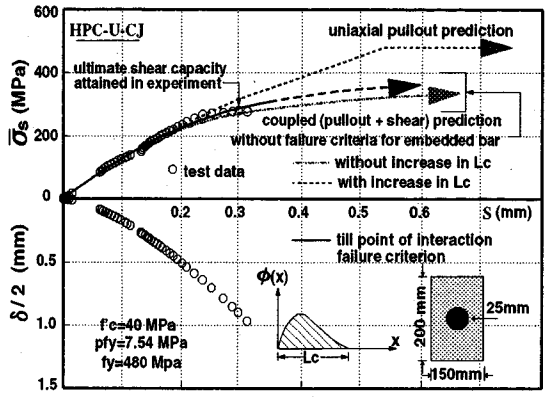

Fig.13 Comparison of experimental [16] and predicted mean bar axial stress with associated displacement paths, without limiting failure criteria for bar.

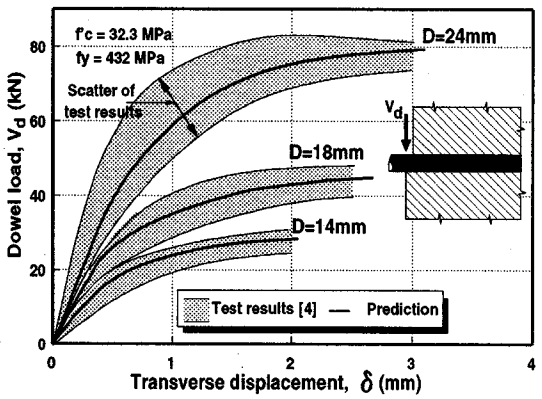

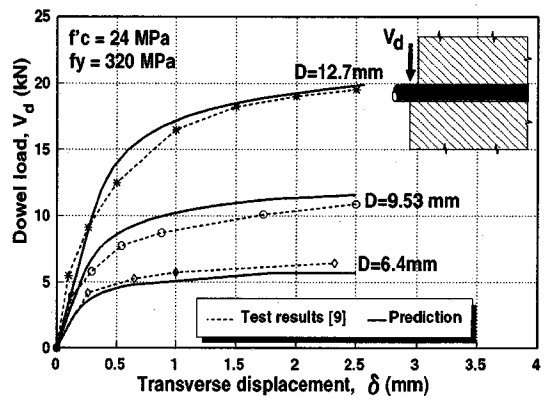

Fig.14 Prediction of dowel load-displacement relation of test results [4), 9)].

In general, the steeper the displacement path, in terms of δ_b/S, brought about by increased reinforcement ratio, flatter interface geometry or lower concrete strength, the lower the mean axial stress, that is attained, as evident through **Fig.11** (Specimens 3,6,8, respectively).

In order to clearly understand the significance of the interaction failure criterion introduced in Eq.(28) of the proposed model, a case is analyzed for a typical test specimen without considering any failure criteria for the bar, other than fracture of the extreme fibers at the end of strain hardening. The results of such an analysis is shown in **Fig.13**. Two cases, with and without the consideration of an increase in curvature zone, L_c, are computed, to check the sensitivity of this proposal in the model. It can be seen that without the definition of a failure criteria, the bar pullout continues to increase with small increase in axial stress, thereby reducing the pullout stiffness.

Test results however do not indicate such high bar pullout values. Therefore the good correlation obtained with test data, for both bar axial capacity and associated pullout at interface, under coupled displacement paths, with the use of the interaction failure criterion, allows it to be considered as an acceptable failure condition in the proposed model. The sensitivity of the increase in L_c in the simulation shown in **Fig.13**, indicates that the relaxation of the supporting concrete spring properties reduces the rate of increase of the curvature at a particular location and the bar axial stresses attained for a given pullout level are increased. However, till the point of the observed experimental bar capacity, the effect of the increase in L_c on the bar axial stress versus pullout relation is not so much.

(3) Force-displacement relationship of embedded bar under pure transverse loads

The behavior of an embedded bar under pure transverse loads, termed as dowel action, have also been experimentally investigated by several researchers[4),6)]. The proposed generic model for the embedded bar can be applied in the case of pure transverse displacements also to predict dowel

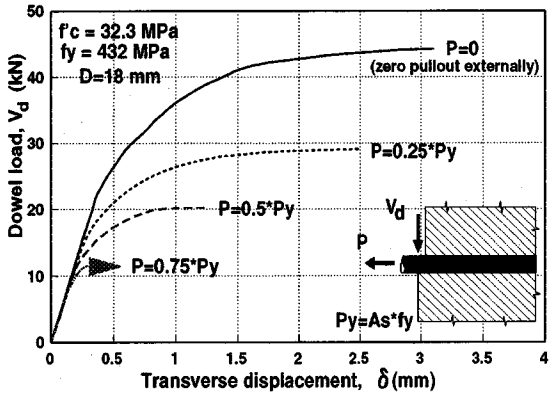

Fig.15 Effect of axial force on dowel load-displacement behavior (computation).

capacity and load displacement relationships. In the absence of any axial pullout, the nonlinearity in the bar under pure shear is much higher than in the case of a bar subjected to a coupled displacement path.

The failure mode is highly ductile with a large spread of plastic strains along the bar axis and large plasticized depths across the bar section. The presence of a zone of localized curvature is also witnessed under this condition[4], similar to that witnessed for tests conducted in this study for coupled displacement paths. Comparison of test [4] and predicted results for bars of different diameters are shown in **Fig.14**, and show good agreement.

Predictions are also attempted for test data from reference (9), with different bar size diameters and different bar and concrete material properties from (4). Predictions obtained are again in good agreement with the test data, as shown in **Fig.14**, which verifies the versatility of the proposed bar model, not only for prediction of mean bar axial stress versus pullout behavior coupled with transverse displacement, but also for the prediction of bar shear stress versus transverse displacement in the absence of any axial pullout. Thus the formulated two dimensionally idealized generic bar model can be used for predicting successfully the axial and transverse bar behavior under any arbitrary coupled or uncoupled displacement path.

Since the validity of the bar model has been verified through a wide range of test results, it can be used to numerically simulate the effect of varying axial force on the reduction of dowel capacity, the possibility of which was raised by Suzuki et al.[11].

Although their test results show considerable scatter and higher dowel capacities than observed in other test results [4),9)], probably due to insufficient cut-off of aggregate interlock, the qualitative trends of reduced dowel capacity with increasing axial force was observed. Computational results of dowel load-transverse displacement behavior in the presence of varying axial force are shown in **Fig.15**.

From the computed results, it is observed that under small axial force, the main source for the stiffness degradation of the dowel behavior is the inelasticity of the supporting concrete due to increasing transverse displacement, which induces higher bearing pressure. This becomes more and more severe in the presence of higher axial forces, and the stiffness degradation is accelerated. Under very high axial force, close to the axial capacity of the bar, the limit condition of maximum interactive stresses govern the ultimate dowel capacity.

5. CONCLUSIONS

Based on new experimental findings of microscopic bar behavior, as extracted from the mechanics of a RC interface, a generic model for embedded bar has been formulated in this study. The model formulation follows rational micro and macro concepts and verification with test data were conducted for each governing step. Following are the general conclusions reached within this scope.

1) By utilizing two basic proposals, based on experimental results, of a 'Bond Deterioration Zone' and a 'Curvature Influencing Zone', coupled with a compatibility relation to predict curvature from transverse displacement, the internal stresses and strains (both along the bar axis and across its section) along with the entire system of forces acting on a bar embedded in concrete, subjected to coupled pullout and transverse shear slip, can be computed.

2) The compatibility relation between bar curvature and the normal displacement of the bar can be established using the Euler-Kirchoff hypothesis of plane sections, and is verified with experimental results, by predicting transverse shear displacement of the bar from its curvature distribution.

3) The reduced axial stiffness of the bar can be computed from the initiation of localized plasticity in the reinforcing bar inside concrete, even as the section at the interface is in purely elastic state. The progressive reduction of axial stiffness, due to gradually increasing plasticity both along the bar axis and across the bar section, with increasing shear displacement, can be predicted for test data.

4) The maximum axial confining stress attained in the reinforcing bar at the interface can be predicted by considering the ultimate interactive stress possible at the maximum curvature location, due to combined axial and bending stresses.

5) The proposed model can also predict the capacity and load-displacement behavior of an

embedded bar under pure transverse displacement paths. This makes the model a generic one applicable under any displacement paths, such as pure axial pullout, pure transverse displacement or arbitrary combination of the two.

6) The proposed model has been independently verified when displacement paths are used as input parameters. For versatile applicability, the prediction of stress transfer behavior of a RC interface, by combining with an aggregate interlock model, needs to be established. Since the evaluation of shear force acting on the bar at the interface, i.e. dowel shear, can be computed from the model, it can be added to the aggregate interlock model to obtain the total shear transferred at the interface by both mechanisms in an unified manner.

For future development, the proposed model is required to cover more generic conditions in reinforced concrete members, in which reinforcing bars are closely arranged, adjacent cracks are introduced with smaller spacing and so on.

REFERENCES

1) Maekawa, K., Mishima, T., Khan, J. and Qureshi, J.: Reduced axial stiffness of deformed bars under shear slip along crack in concrete, *CEB conference,'Bond in Concrete'*, 1993.
2) Shima, H., Chou, L. and Okamura, H.: Micro and macro model for bond behavior in reinforced concrete, *Journal of the faculty of engineering, University of Tokyo (B)*, Vol. 39, No.2, 1987.
3) Bujadham, B., Maekawa, K. and Mishima, T.: Cyclic discrete crack modelling for reinforced concrete, *Computer aided analysis and design of reinforced concrete structures*, Pineridge Press, pp. 1225-1236, 1990.
4) Poli, S. D., Prisco, M. D. and Gambarova, P. G.: Shear response, Deformations, and subgrade stiffness of a dowel bar embedded in concrete, *ACI Structural Journal*, V. 89, No. 6, pp.665-675, 1992.
5) Mishima, T., Yamada, K., and Maekawa, K.: Localized deformational behavior of a crack in RC plates subjected to reversed cyclic loads, *Proc. of JSCE*, No. 442/V-16, pp.161-170, 1992.
6) Sourishian, P., Obaski, K., Rojas, M. C. and Sim, J.: Analysis of dowel bars acting against concrete core, *ACI Journal*, Proceedings V.83, No. 4, pp.17-42., 1986.
7) Ueda, T., Lin, I. and Hawkins, N. M.: Beam bar anchorages in exterior column beam connections, *ACI Journal*, pp.412-422, 1986.
8) Tani, S.: Inelastic analysis of R/C frame structures, *Proc. of ASCE*, Vol. 100, ST7, pp.1433-1449, 1974.
9) Paulay, T., Park, R. and Phillips, M. H.: Horizontal Construction Joints in Cast-In-Place Reinforced Concrete, Shear in Reinforced Concrete, *ACI Publication SP* 42-27, Vol.2, pp. 599-616, 1974.
10) Izumo, J., Shima, H. and Okamura, H.: Analytical Models for RC Panel Elements Subjected to In-Plane Forces, *Concrete Library of JSCE*, No. 12, pp. 155-181, 1989.
11) Suzuki, M., Nakamura, T., Horiuchi, M. and Ozaka, Y: Experimental Study on the Influence of Tension Force on Dowel Effect of Axial Bars, *Proceedings of the JSCE*, No. 426/V-14, pp. 159-166, 1991. (In Japanese)
12) Okamura, H. and Maekawa, K.: *Nonlinear Analysis and Constitutive Models of Reinforced Concrete*, Gihodo-Press, Tokyo, 1991.
13) Beedle, S. L., Ready, J. A. and Johnston, B. G.: Tests of Columns under Combined Thrust and Moment, *Proc. of Society of Experimental Stress Analysis*, Vol. 8, pp. 109-132, 1950.
14) Khalil, H. S. and Tadros, G. S.: Plastic Resistance of Mild Steel Rectangular Sections, *The Structural Engineer*, No. 7, Vol. 51, pp. 239-249, 1973.
15) Park, R. and Paulay, T.: *Reinforced Concrete Structures*, Wiley Interscience Publication, pp. 38, 1975.
16) Maekawa, K. and Qureshi, J.: Embedded bar behavior in concrete under combined axial pullout and transverse displacement, *Proc. of JSCE*, No.532/V-30, pp.183-195, 1996.

(Received May 31, 1995)

軸引張とそれに直交する変位を同時に受ける鉄筋の計算モデル

前川宏一・Juneid QURESHI

本研究は，鉄筋軸に直交する変位と引抜けを同時に受ける一般的な載荷条件下において，鉄筋の挙動を代表する計算モデルを提案するものである．鉄筋軸に直交する変位と鉄筋軸に沿って分布する曲率との間に成立する適合条件を用いて，せん断ひび割れや接合部を交差する鉄筋に現れる塑性変形の局所化を定量化した．これによって，鉄筋がダウエル作用を受けた時に，鉄筋軸方向の引抜け剛性と定着耐力が低下する機構を説明することに成功した．

米国ITASCA（イタスカ）社開発の岩盤・地盤解析プログラム

未来設計企業 CRC

UDEC 3DEC 個別要素法(DEM)プログラム

個別要素法（離散要素法）は、1971年にDr.P.Cundallが発表した不連続体数値解析手法であり、岩盤や地盤をブロックや土粒子の要素の集合体と考え、個々の要素が隣接要素から受ける力により運動方程式にもとづき挙動する様子を時間差分式にて時刻繰返し計算する手法です。個別要素法は不連続力学の中心手法として位置づけられ、岩盤・地盤の崩落や安定性の解析、大深度地下空間、核廃棄物地下処理、鉱物資源開発等のプロジェクトおよび粒状体力学（粉体工学）の分野で有力な解析手段となっています。現在UDEC，3DECは全世界の研究機関・企業で標準コードとして広く使用されています。

オプション

■Barton-Bandisモデル

適用分野

- ●粒状物質の挙動解析
- ●鉱山採掘等　掘削解析
- ●地震応答解析
- ●ジョイント内流れ解析（浸透連成：UDEC）
- ●核廃棄物の熱応力解析（熱連成：UDEC）

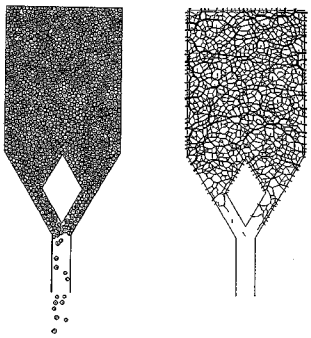

ホッパー内粒状体挙動解析

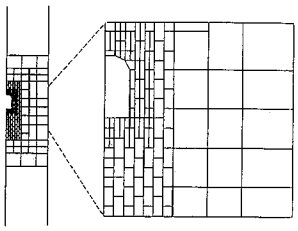

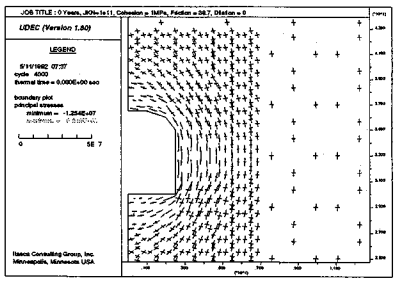

核廃棄物地中処理影響解析

■販売条件

UDEC・3DEC・FLAC

- ◆EWS（SUN-SPARC）
- ◆IBM-PC/AT及び互換機
- ◆UDECはソースコードで提供します。
- ◆3DEC・FLACはロードモジュールで提供します。

亀裂性岩盤の3次元掘削解析

FLAC 有限差分法(FDM)プログラム

FLACは個別要素法コードUDEC，3DECを発表したDr.P.Cundallが同様の有限差分ロジックを用いて連続体の塑性大変形の解析するために開発したコードで、現在、全世界で数多く使用されています。有限差分法は、地盤、岩盤を有限な領域内で離散化し、連動方程式と構成則を差分方程式として解析するもので、有限要素法に比べ非線形大歪が扱えることで大きな優位性を持っています。

FLACは小一大歪　非線形、動的一静動挙動を始めとし、豊富な機能　オプションを備えたPC、ワークステーション用の地盤解析コードです。

オプション

- ■ダイナミック解析モデル
- ■クリープ解析モデル
- ■熱解析モデル

適用分野

- ●斜面・盛土の設計、安定解析
- ●浅／深基礎設計
- ●アースダム、コンクリートダムの設計
- ●トンネルの設計
- ●核廃棄物貯蔵解析
- ●液状化解析

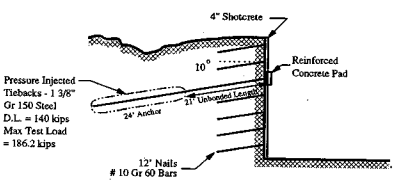

地盤安定解析

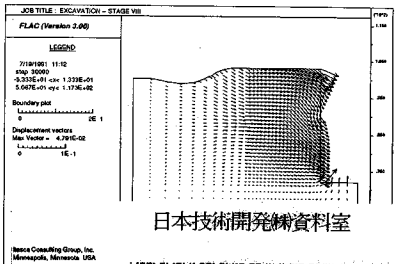

日本技術開発㈱資料室

株式会社CRC総合研究所

●西日本事業部　科学システム
〒541 大阪市中央区久太郎町

●科学システム事業部　営業
〒136 東京都江東区南砂2-7

土と水の連成逆解析プログラム

未来設計企業 CRC

UNICOUP

応力解析と浸透解析がドッキングした!

軟弱地盤の解析に!

海洋開発・埋立

盛土・掘削

出力項目

- 各節点での変位、各要素での応力
- 各節点での全水頭・圧力水頭 他
- 豊富な図化処理
  変位図、変位ベクトル図、応力ベクトル図、応力コンター図、安全率コンター図、水頭コンター図、圧力水頭コンター図

プログラムの特長

- 応力と地下水の流れをカップルさせた問題が解析可能です。(圧密含む)
- 地下水の流れは飽和・不飽和域を対象としています。
- 多段掘削・盛土や降雨等が扱えます。
- 梁や連結要素も扱え実用的です。
- 経時観測記録(変位・水位)があれば、非線形最小二乗法に基づき変形係数や透水係数が逆解析できます。(順解析、逆解析がスイッチにて選択可能です。)
- 弾性・非線形弾性・弾塑性・弾粘塑性を示す地盤が扱えます。
  非線形弾性(電中研式、ダンカン・チャンの双曲線モデル)
  弾塑性(ドラッガー・プラガー、モール・クーロン、カムクレイモデル、ハードニング、ソフトニング)
  弾粘塑性(関口・太田モデル)

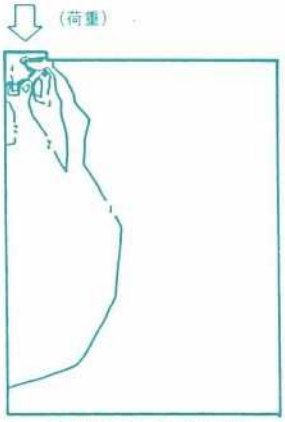

応力増分コンター($d\sigma_V$)
(10日後)

変位ベクトル図(40日後)

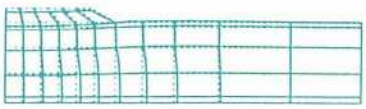

盛土(40日)後の地盤の変形

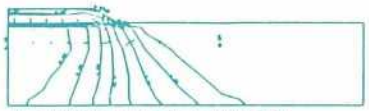

盛土(40日)後の地下水の流れと水頭コンターおよび自由水面

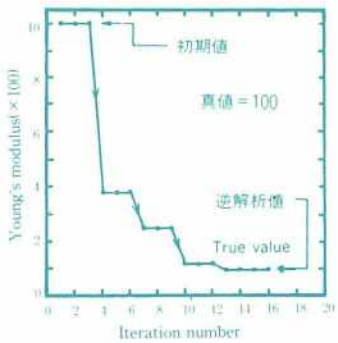

ヤング率と繰り返し回数の関係

逆解析によるパラメータの推定

この製品は、情報処理振興事業協会の委託を受けて開発したものです。
通商産業省 特別認可法人
IPA 情報処理振興事業協会

株式会社 CRC総合研究所

●西日本事業部　科学システム営業部／担当：岩崎
〒541 大阪市中央区久太郎町4-1-3 TEL:06- 241-4121

●科学システム事業部　営業第1部／担当：澤村
〒136 東京都江東区南砂2-7-5　TEL:03-5634-5790